

Pressure-induced amorphization of noble gas clathrate hydrates

Paulo H. B. Brant Carvalho^{1,*}, Amber Mace,² Ove Andersson³, Chris A. Tulk,⁴ Jamie Molaison,⁴ Alexander P. Lyubartsev,¹ Inna M. Nangoi⁵, Alexandre A. Leitão,⁵ and Ulrich Häussermann¹


¹Department of Materials and Environmental Chemistry, Stockholm University, SE-10691 Stockholm, Sweden

²Department of Chemistry—Ångström Laboratory, Uppsala University, SE-75236 Uppsala, Sweden

³Department of Physics, Umeå University, SE-90187 Umeå, Sweden

⁴Chemical and Engineering Materials Division, Oak Ridge National Laboratory, Oak Ridge, Tennessee 37831, USA

⁵Department of Chemistry, Federal University of Juiz de Fora, Juiz de Fora-MG, 36036-900, Brazil

 (Received 5 October 2020; revised 19 January 2021; accepted 25 January 2021; published 17 February 2021)

The high-pressure structural behavior of the noble gas (Ng) clathrate hydrates Ar · 6.5 H₂O and Xe · 7.2 H₂O featuring cubic structures II and I, respectively, was investigated by neutron powder diffraction (using the deuterated analogues) at 95 K. Both hydrates undergo pressure-induced amorphization (PIA), indicated by the disappearance of Bragg diffraction peaks, but at rather different pressures, at 1.4 and above 4.0 GPa, respectively. Amorphous Ar hydrate can be recovered to ambient pressure when annealed at >1.5 GPa and 170 K and is thermally stable up to 120 K. In contrast, it was impossible to retain amorphous Xe hydrate at pressures below 3 GPa. Molecular dynamics (MD) simulations were used to obtain general insight into PIA of Ng hydrates, from Ne to Xe. Without a guest species, both cubic clathrate structures amorphize at 1.2 GPa, which is very similar to hexagonal ice. Filling of large-sized H cages does not provide stability toward amorphization for structure II, whereas filled small-sized dodecahedral D cages shift PIA successively to higher pressures with increasing size of the Ng guest. For structure I, filling of both kinds of cages, large-sized T and small-sized D, acts to stabilize in a cooperative fashion. Xe hydrate represents a special case. In MD, disordering of the guest hydration structure is already seen at around 2.5 GPa. However, the different coordination numbers of the two types of guests in the crystalline cage structure are preserved, and the state is shown to produce a Bragg diffraction pattern. The experimentally observed diffraction up to 4 GPa is attributed to this semicrystalline state.

DOI: [10.1103/PhysRevB.103.064205](https://doi.org/10.1103/PhysRevB.103.064205)

I. INTRODUCTION

Clathrate hydrates are crystalline compounds consisting of a framework of tetrahedrally coordinated water molecules forming polyhedral cages which include guest species [1]. These guest species are rather diverse and can range from smaller-sized organic molecules [e.g., natural gas, tetrahydrofuran (THF)], linear and bent triatomic molecules (such as carbon dioxide and H₂S), diatomic molecules (e.g., hydrogen, nitrogen, chlorine), to single atom noble gases (Ngs) [2,3]. Clathrate hydrate structures are stabilized by hydrogen bonds between water host molecules and van der Waals forces between host and guest [4]. These guest-host interactions determine the type of crystalline structure that may form: most clathrate hydrates exist in one of two cubic structures [1], termed structure I (CS-I, *Pm-3n* space group, lattice parameter $a \approx 12$ Å) [5] and structure II (CS-II, *Fd-3m* space group, lattice parameter $a \approx 17$ Å) [6,7]. Other frameworks have

been either predicted theoretically or attained experimentally at high pressures [8–15].

The two cubic framework structures feature two types of polyhedral cages each (see Fig. 1). The unit cell of CS-I contains 46 water molecules which build up two dodecahedral 5¹² cages (D cages) and six tetrakaidecahedral 5¹²6² cages (T cages). The unit cell of CS-II contains 136 water molecules which build up 16 dodecahedral D cages and 8 hexakaidecahedral 5¹²6⁴ cages (H cages) [16]. The composition of cubic clathrate hydrates is variable: sometimes the smaller-sized D cages are not occupied, or more frequently, both types of cages are occupied but not completely. In this case, typical occupancies are between 0.8 and 0.9. Several types of clathrate hydrates occur abundantly in nature and are considered future energy resources (or environmental threats) due to large amounts of stored natural gas [17]. Apart from their potential significance in gas or energy storage and transport, clathrate hydrates have been discussed for application in carbon capture and storage, water desalination, separation of ionic liquids, and food and pharmaceutical engineering [1,18–21].

Most central to clathrate hydrates is an understanding of the guest-host interactions. These interactions are particularly sensitive to density, and it has been shown that pressure is a valuable variable for probing intermolecular interaction potentials and hydration structures of guest species [22]. Investigations of cubic clathrate hydrates at high pressure

*paulo.barros@mmk.su.se

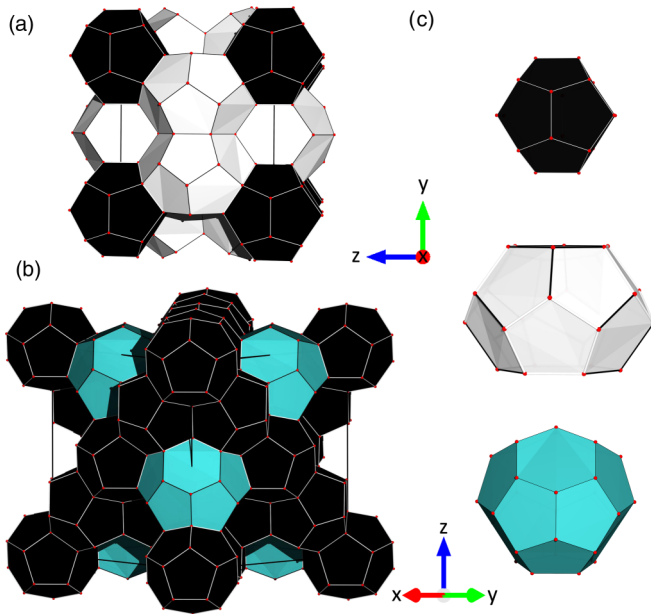


FIG. 1. Unit cell of the cubic clathrate hydrate structures. (a) CS-I ($Pm\bar{3}n$, $a \approx 12 \text{ \AA}$), composed of 46 water molecules forming a hydrogen-bonded network around six large T cages (gray) and two small D cages (black). (b) CS-II ($Fd\bar{3}m$ space group, lattice parameter $a \approx 17 \text{ \AA}$), composed of 136 water molecules which build up 16 D cages and eight H cages (cyan). (c) The three different cages in cubic structured clathrate hydrates: D cages (pentagon dodecahedra, 5^{12}), common for both CS-I and CS-II; T cages (tetrakaidecahedra, $5^{12}6^2$), large cages in CS-I; and H cages (hexakaidecahedra, $5^{12}6^4$), large cages in CS-II (and largest among all). T cages are represented in (c) with their two different types of pentagon faces: those constituting H cages only (black edges), and those constituting both H and D cages (white edges). Red spheres on cage vertexes represent oxygen atoms.

(in the gigapascal regime) and close to room temperature (260–280 K) have led to the observation of new types of hydrate frameworks, both of clathratic nature and filled-ice structures [8,9]. The high-pressure hydrates have typically more guest-rich compositions than the original cubic clathrate hydrates since they follow from decomposition of the latter. The structure of high-pressure hydrates and phase diagrams are discussed in the literature [8,9,12–15,22–26]. When compressed at lower temperatures (below 135 K), cubic clathrate hydrates exhibit instead a sharp, first-order-like transition to an amorphous state, analogous to pure water’s high-density amorphous (HDA) ice, which is obtained when pressurizing hexagonal ice I_h at similarly low temperatures [26]. Since the tetrahedral nearest neighbor arrangement of water molecules in the host structure of cubic clathrate hydrates is identical to ice I_h and the concentration of the guest is rather small, their pressure-induced amorphization (PIA) should follow the same or a very similar mechanism. However, since examples of cubic clathrate hydrates displaying PIA are rather limited, this is still not clear. Likewise, structural and physical properties of the amorphous forms are largely unexplored.

Noble gas clathrate hydrates were targeted early on as model systems for the statistical thermodynamic analysis of clathrate hydrates [4]. This is because monoatomic Ngs are distinguished in their isotropic interactions with the hosting

water cage, which are easy to model, and by providing a homologous series of increasingly larger (and heavier) guests. Studies can then systematically address effects of guest size and cage occupancy to clathrate hydrate stability. Consequently, Ng clathrate hydrates also represent ideal model systems for studying the PIA phenomenon. We selected Xe and Ar clathrate hydrate, which adopt the CS-I and CS-II structure, respectively, as prototypical systems. Their composition has been reported as $\text{Ar} \cdot 6.5 \text{ H}_2\text{O}$ (D 89% filled and H 83%) and $\text{Xe} \cdot 7.2 \text{ H}_2\text{O}$ (D 76% filled and T 81%) [6,23,24]. The near room temperature high-pressure behavior is also well studied [9]. With increasing pressure, CS-II Ar hydrate (AH) transforms successively into a hexagonal, tetragonal, and orthorhombic clathrate structure variant. The latter is stable up to 6 GPa, after which decomposition into solid Ar and ice VII occurs [8–11]. CS-I Xe hydrate (XH) was found stable up to about 1.7 GPa. At higher pressure, the phase undergoes a transition to the hexagonal clathrate structure (which can be recovered to ambient pressure at 77 K in the slightly modified HS-I structure) [12]. Above 2.9 GPa, the hexagonal clathrate structure decomposes into solid Xe and ice VII [13–15]. With respect to high-pressure investigations at low temperatures (i.e., below 135 K), nothing is known about Ar clathrate hydrate, whereas CS-I XH was included in the seminal study by Handa *et al.* [27]. These authors performed piston cylinder experiments on CS-II THF, SF_6 hydrates, and CS-I XH at 77 K and up to 1.7 GPa. It was found that the CS-II type clathrate hydrates amorphized, whereas XH did not undergo any transformation in the applied pressure range. However, recent potential energy minimization calculations (using empirical potentials) considering fully occupied CS-I Ng hydrate for $\text{Ng} = \text{Ar}, \text{Kr}, \text{and Xe}$ predicted PIA at 1.8, 2.6, and 4 GPa, respectively (referring to 0 K) [28].

In this paper, high-pressure neutron powder diffraction (NPD) experiments were carried out on CS-II AH and CS-I XH for pressures from 0.1 to 5 GPa at 95 K. Both clathrate hydrates were found to collapse into an amorphous state. The PIA behavior was then examined with molecular dynamics (MD) simulations, addressing the complete series of Ng atoms, Ne through Xe.

II. EXPERIMENTAL DETAILS AND METHODS OF ANALYSIS

A. NPD experiments

A range of NPD experiments involving several samples of Ar and Xe clathrate hydrates were conducted at the SNAP beamline at the Spallation Neutron Source (SNS), Oak Ridge National Laboratory (ORNL), USA. All samples were synthesized onsite on a setup put in place at SNAP. Data from 10 experiments were combined in this paper, and details to each sample and experiment can be found in the Supplemental Material (SM) [29].

B. Synthesis of XH

Fully deuterated CS-I Xe clathrate hydrate was synthesized similarly to the procedure described in Ref. [27]. Finely ground and sieved ($<45 \mu\text{m}$ particles) D_2O ice (99.9% deuterated, Sigma Aldrich) was prepared and transferred to a cold

pressure vessel, like the gas cell used for the synthesis of ^{36}AH as in Ref. [6]. The vessel was sealed and filled with ~ 50 bar of precooled Xe and kept in a freezer at 250 K for > 10 days. The precursor ice I_h was still found present in all samples (~ 10 to 40% of ice contaminant), possibly due to a synthesis time that was too short. Xe hydrate samples were recovered and stored in LN_2 prior to NPD experiments.

C. Synthesis of AH

Fully deuterated CS-II clathrate hydrate of Ar was synthesized following the procedure described in Ref. [6]. Finely ground D_2O ice (99.9% deuterated, Sigma Aldrich) was prepared and transferred to a cold (below freezing) pressure vessel containing stainless steel ball bearings. The vessel was sealed and filled with 150 bar of precooled Ar. The vessel was then intermittently tumbled for > 10 days in a freezer at 250 K, providing refreshed grain surfaces for a complete clathrate formation. The complete conversion of ice I_h to the CS-II clathrate was confirmed by powder x-ray diffraction on a Panalytical X'Pert Pro diffractometer using the Anton Paar TTK 450 Low Temperature Chamber. Ar hydrate samples were recovered and stored in LN_2 prior to NPD experiments.

D. In Situ Time-of-Flight NPD

Time-of-flight NPD experiments were performed in the temperature range of 95–220 K using a standard VX Paris-Edinburgh pressure cell with LN_2 -cooled stainless-steel anvils, which can reach up to 10 GPa at temperatures as low as 77 K. Samples were loaded at LN_2 temperature in null-scattering TiZr gaskets, with lead powder added as a pressure marker. The gaskets were pressurized to ~ 0.1 GPa upon loading to stabilize the samples, which warmed up to about 170 K during transferring of the pressure cell to the cryostat, where they were cooled to 95 K. For all samples, a longer (~ 2 h) starting collection of neutron diffractograms at the crystalline stage was done, allowing the refinement of the clathrate hydrate unit cells and identification of contaminants, if any. Pressurization was done in steps of 0.1–0.2 GPa, followed by data collection during 15 min to up to several hours. Samples were compressed until their full amorphization could be observed by the disappearance of all their Bragg diffraction peaks. In addition, vanadium powder and an empty gasket were measured for intensity normalization and for background correction, respectively. Masking of the detector banks was done during data treatment at higher-pressure steps due to partial shading of the detectors by the anvil and press materials.

E. MD Modeling

Simulation cells were constructed using the GenIce software [30], which places oxygen atoms at their crystallographic sites in the cubic unit cell, randomizes the distribution of hydrogen atoms constrained by the Bernal-Fowler ice rules, and chooses the configuration with zero (minimum) net polarization. CS-II supercells consist of $2 \times 2 \times 2$ periodically replicated cubic unit cells consisting of 1088 H_2O molecules with ~ 34 Å initial cell dimensions. CS-I supercells consist of $3 \times 3 \times 3$ periodically replicated cubic unit cells consisting

of 1242 H_2O molecules with ~ 36 Å initial cell dimensions. The guest atoms (Ne, Ar, Kr, Xe) were randomly distributed fulfilling the following compositions: (case i) full occupancies, (case ii) only small (D) cages filled; (case iii) only large (CS-I: T, CS-II: H) cages filled; (case iv, Ne only) CS-II with only H cages doubly occupied, and full occupancy of D cages plus H cages doubly occupied.

The PIA was modeled with isotropic (NPT) MD simulations in the LAMMPS software [31]. To describe the interatomic interaction during the MD simulations, the TIP4P/Ice [32] and UFF [33] force fields were used for ice and Ngs, respectively, and the Lorentz-Berthelot mixing rules were applied. The Nose-Hoover barostat algorithm with the Melchionna modification [34] was employed to control the temperature and pressure of the systems. The simulations were carried out at 95 K, and the pressure was subsequently increased from 1 to 3 GPa in steps of 0.05 GPa. At each pressure step, the system was first incremented gradually over 2 ns; the system was then equilibrated for 5 ns, followed by a further 1 ns simulation during which statistics for the densities and radial pair distribution functions (PDFs) were collected. The simulation time step was 1.0 fs, and barostat relaxation time was set to 2000 time steps.

Snapshots (single frame in a simulation) were taken from 100% CS-I XH and 100% CS-II AH MD calculations at pressure steps just before (CS-I: 2.4 GPa; CS-II: 1.4 GPa) and immediately after collapse (CS-I: 2.6 and 2.9 GPa; CS-II: 1.7 GPa). MD supercells (i.e., $2 \times 2 \times 2$ CS-II and $3 \times 3 \times 3$ CS-I unit cells) were doubled along each axis (now corresponding to $4 \times 4 \times 4$ CS-II and $6 \times 6 \times 6$ CS-I cells) for simulating neutron diffraction patterns by the XaNSoNS software [35].

III. RESULTS AND DISCUSSION

A. PIA of CS-I XH and CS-II AH

Although the synthesis of Xe and Ar clathrate hydrate followed established protocols [6,27], XH samples showed various amounts of ice I_h , whereas AH could be prepared virtually ice-free. For this paper, the presence of ice was deemed to not interfere with obtained results. The composition of the hydrates was assumed to be as earlier determined by Flacau *et al.* [23], $\text{Xe} \cdot 7.2 \text{H}_2\text{O}$ (D 76% filled and T 81%), and Yang *et al.* and Brant Carvalho *et al.* [6,24], $\text{Ar} \cdot 6.5 \text{H}_2\text{O}$ (D 89% filled and H 83%). Figure 2 shows initial neutron diffraction patterns of Xe and Ar clathrate hydrate samples at 95 K and about 0.1 GPa (experiments AH5 and XH2, respectively, see SM for details [29]). For fitting the diffraction data by Rietveld refinement, the structures from Ikeda *et al.* [36] and Brant Carvalho *et al.* [6] were used as the starting models for Xe and Ar clathrate hydrate, respectively. Refined parameters included background and peak profile terms, hydrate/ice content ratio and unit cell parameters. As a general procedure, the samples were first isothermally compressed at 95 K until a structural change, i.e., amorphization, occurred. Afterwards, various p,T pathways were pursued to check the reversibility of observed transitions. These pathways are depicted in Fig. 3, and below, we summarize findings (see SM for details to specific AH and XH experiments [29]).

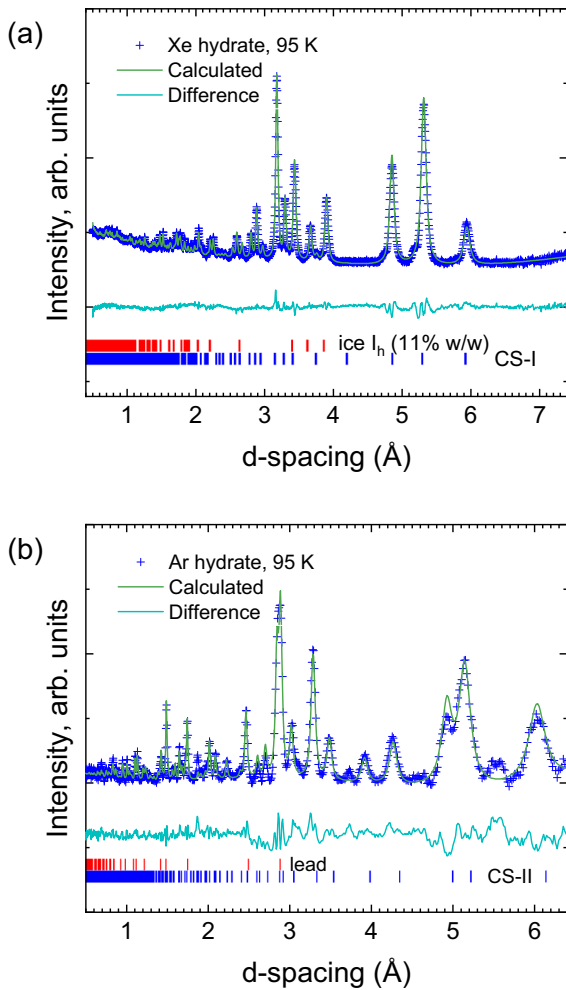


FIG. 2. Experimental neutron powder diffraction (NPD) profiles of (a) CS-I Xe and (b) CS-II Ar clathrate hydrate. The diffractograms were measured at 95 K and at the lowest pressure point 0–0.1 GPa. Profiles obtained upon Rietveld refinement are shown as solid lines. The difference curves are plotted beneath. Tick marks show Bragg positions of allowed reflections for the fitted phases. Xe hydrate: $a = 11.8662(6)$ Å, $R_{wp} = 3.73\%$, $\text{GoF} (\chi^2) = 3.04$. Ar hydrate: $a = 17.040(3)$ Å, $R_{wp} = 1.37\%$, $\text{GoF} (\chi^2) = 2.90$.

During compression, the hydrate phases were consistent with the structure in the literature, despite the peak broadening caused by strain effects. CS-I XH was observed to be stable at 95 K up to 4.0 GPa, and CS-II AH up to 1.4 GPa. Beyond these pressures, both hydrates transformed into amorphous states. The PIA was characterized by the complete disappearance of all Bragg diffraction peaks of a given phase. A representative evolution of the diffraction patterns with pressure is shown in Fig. 4. The behavior of CS-II AH appears very similar to earlier investigated CS-II hydrates (i.e., THF, 1,3-dioxolane, cyclobutanone, acetone [37], SF_6 [27]), for which amorphization was observed in a pressure range of 1.2–1.6 GPa at similar temperatures. This is at slightly higher pressures than the pressure of the ice I_h -to-HDA transition (~ 1 GPa) [26]. In contrast, the PIA of CS-I XH occurred at considerably higher pressures. There is only one more example of a CS-I hydrate

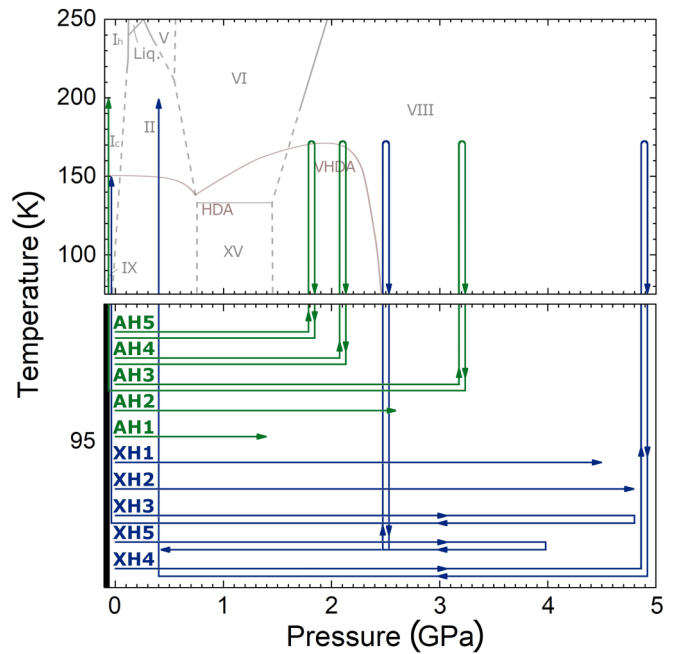


FIG. 3. Experimental pathways followed in this paper. The phase diagram of pure ice (from Salzmann, Ref. [54]) is underlaid as background. Ar hydrate (AH) experiments (green), AH1: Compression to PIA (1.4 GPa); AH2: Compression to 2.6 GPa; AH3: Compression to PIA and up to 3.15 GPa, temperature cycling to 170 K, cooling, decompression, and heating to 200 K at ambient pressure; AH4: Compression to 2 GPa, temperature cycling to 170 K, cooling, and decompression; AH5: Compression to 1.9 GPa, temperature cycling to 170 K, cooling, and decompression. Xe hydrate (XH) experiments (navy blue), XH1: Compression to 4.5 GPa; XH2: Compression to 4.8 GPa; XH3: Compression to 5.1 GPa, decompression to atmospheric pressure, and heating to 150 K; XH4: Compression to 4.9 GPa, temperature cycling to 170 K, cooling, decompression to 0.4 GPa, and heating to 200 K; XH5: Compression to 4 GPa, decompression to 2.5 GPa, heating to 170 K, and cooling back to 95 K, decompression to 0.48 GPa.

which has been studied by low temperature compression: CH_4 hydrate was pressurized to 3.2 GPa at 100 K, resulting in an amorphous sample. Although the pressure for PIA was not precisely determined in this experiment, it indicates that CS-I hydrates amorphize at higher pressures than CS-II hydrates.

To investigate the reversibility of PIA, the amorphous hydrates were then brought back to atmospheric pressure at temperatures near 100 K. Unlike HDA ice (but like THF and other CS-II hydrates), both amorphous clathrate hydrates recrystallize upon low temperature decompression. In another experiment, we temperature cycled the amorphized hydrates to ~ 170 K at a pressure above the amorphization pressure, following the procedure from Suzuki [38] and Bauer *et al.* [39]. This procedure has been shown to produce a recoverable, denser amorphous form for several CS-II hydrates [38–41], which correlates to the “very HDA” form of water ice [42]. Indeed, after temperature cycling, amorphous AH did not recrystallize when recovered to ambient pressure at 95 K (experiments AH3–5, SM [29]). Upon heating the recovered amorph, recrystallization was seen at 120 K. At 150 K, the

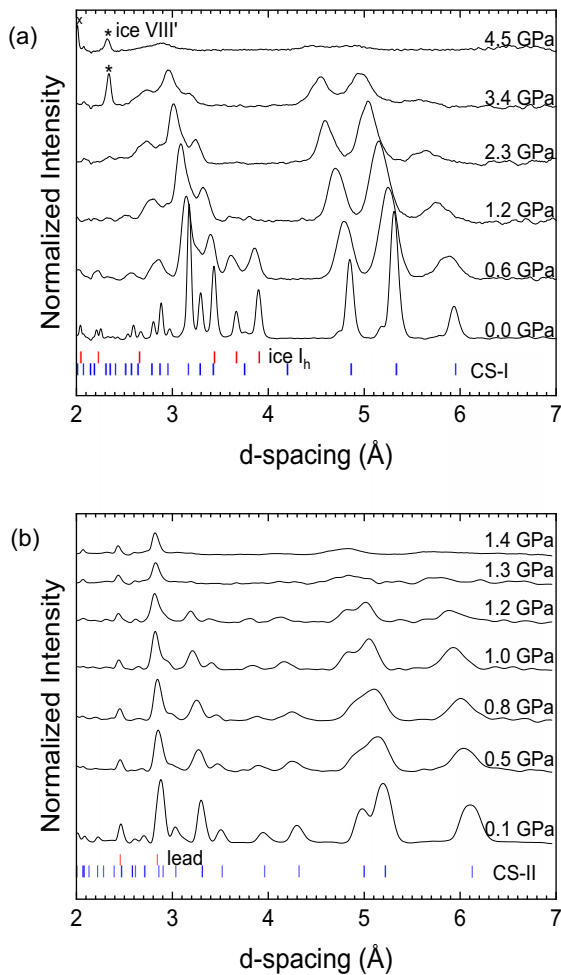


FIG. 4. Evolution of the neutron powder diffraction (NPD) profiles of (a) CS-I Xe and (b) CS-II Ar hydrate upon compression. Tick marks show Bragg positions of allowed reflections for the fitted phases. Stars mark peaks from ice (111 reflection of ice VII or 112 reflection of ice VIII), which can be seen in (a) after recrystallization of high-density amorphous (HDA) above 2.5 GPa. Cross marks the 110 peak of iron as the steel anvil shades part of the beam at high pressures. Patterns were treated for background (including diffuse scattering from the samples) and smoothed for clarity.

clathrate hydrate sample decomposed to Ar and ice I_h , in agreement with earlier observations [43]. In contrast, amorphous XH recrystallized in all attempts of recovery from high pressures. As a matter of fact, crystalline features from the CS-I phase were already observed at ~ 3 GPa on decompression (Fig. S1, SM [29]). The recrystallized XH samples were carefully investigated for their ice content. As a reminder, XH samples contained various amounts of I_h , which upon compression at 95 K forms HDA at around 1 GPa and then recrystallizes as ice VIII' above 2.5 GPa [see Fig. 4(a)] [44]. On pressure release, I_h reforms. We did not find a significantly changed volume fraction of I_h with respect to the starting samples (differences were below 4%), which indicates that recrystallized XH and most likely also its amorphous form have the same composition. We infer that amorphous AH and XH behave differently with respect to their recoverability to ambient pressure, but we cannot entirely rule out that crystalline

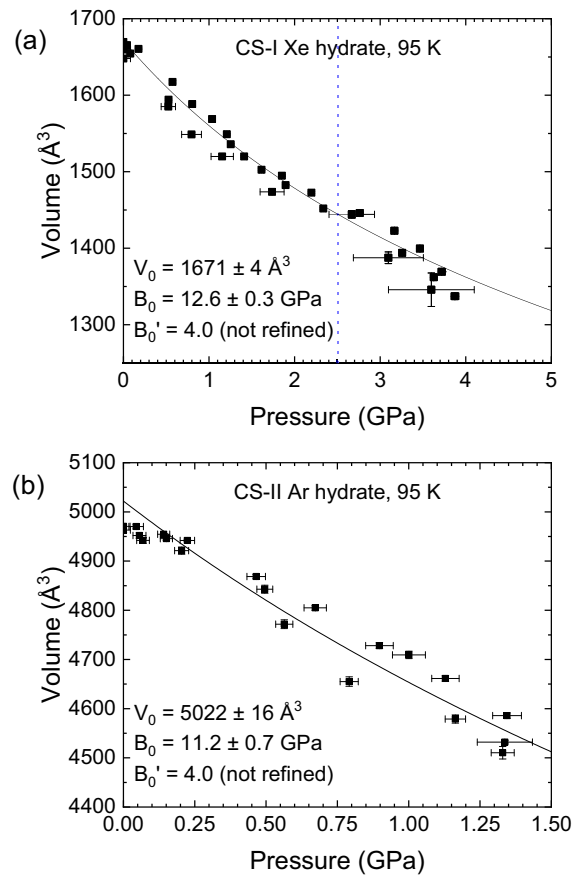


FIG. 5. Equations of state at 95 K of (a) Xe hydrate and (b) Ar hydrate. The line is a fit of the Murnaghan equation $V_0/V = [p(B'/B) + 1]^{1/B'}$ with V_0 , B , and B' being the volume at zero pressure, the bulk modulus, and its first pressure derivative, respectively. The dashed line in (a) marks a transition to a semicrystalline state, as suggested from molecular dynamics (MD) simulations.

domains of ice VIII' influence the recrystallization behavior of amorphous XH.

B. Equation of states of CS-I XH and CS-II AH and analysis of their PIA behavior

The diffraction patterns provide the evolution of the hydrate lattices with increasing pressure, which were used to calculate the equation of state (EoS) of the two hydrates at 95 K. For this, we used the simple Murnaghan relation $V_0/V = [p(B'/B) + 1]^{1/B'}$, with V_0 , B , and B' being the volume at zero pressure, the bulk modulus, and its first pressure derivative, respectively [45]. (Note that strictly the Murnaghan relation is only valid for hydrostatic conditions, which are not fulfilled in our experiments.) The obtained EoS are shown in Figs. 5(a) and 5(b). The extrapolated ambient pressure lattice parameters are within experimental error of those reported in the literature: CS-I XH: $a_0 = 11.87(52)$ Å; CS-II AH: $a_0 = 17.12(84)$ Å [46]. The bulk modulus for CS-I XH is 12.7(3) GPa in the 0–4 GPa pressure range, and the one for CS-II AH is 11.2(7) GPa in the 0–1.4 GPa range. We note that a previous determination of the bulk modulus for XH at room temperature and for the pressure interval of its stability at this

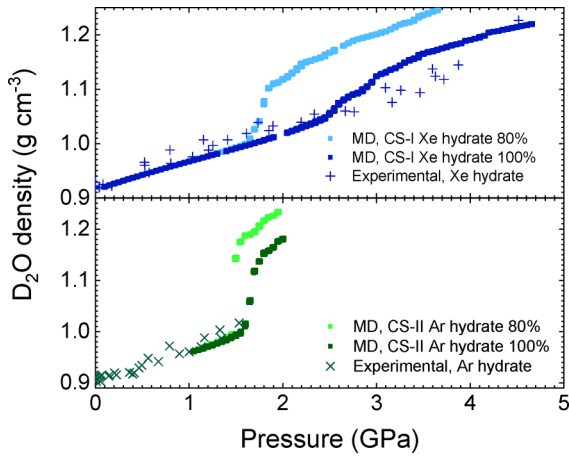


FIG. 6. Density vs pressure comparison from neutron powder diffraction (NPD) experiments and molecular dynamics (MD) simulations. CS-I Xe hydrate (top) and CS-II Ar hydrate (bottom). MD data were rescaled for D_2O , from simulations of cage occupancies ideally fully occupied (100%) and approaching the experimental composition: 80% of D and T cages filled in Xe hydrate, 80% of D and H cages filled in Ar hydrate.

temperature 0–1.5 GPa yielded a value of 9.3(4) GPa [15,47] (whereas the one of AH, in the pressure range 0–0.7 GPa, does not seem to be determined). Manakov *et al.* recently showed that the bulk moduli of CS-I and CS-II hydrates at room temperature, in most cases, were close to each other with $B = 9(2)$ GPa and are mainly determined by the elasticity of the hydrogen-bonded framework [47].

Figure 6 shows the MD calculated density for Xe and Ar clathrate hydrate, rescaled for D_2O , at 95 K as a function of pressure. For the simulations, we considered two scenarios, fully occupied cages and a random 80% occupancy for both types of cages. The latter scenario should correspond closely to the experimental composition. The compressibility of the crystalline forms is in good agreement with the experimental values. For Ar clathrate hydrate, the calculated density increases discontinuously above 1.4 and 1.6 GPa for the 80 and 100% occupied cases, respectively, which signals the onset of amorphization. This is in very good agreement with the experimentally observed amorphization pressure. We note that full occupancy of cages slightly increases the amorphization pressure, i.e., stabilizes the CS-II clathrate, and we will return to this subject later.

At first sight, the MD calculated and experimentally observed compression behavior for CS-I XH do not seem to agree well. The MD simulations predict amorphization above 1.6 and 2.5 GPa for the 80 and 100% occupied cases, respectively. In the experiment, however, Bragg diffraction is clearly present up to at least 4 GPa [cf. Fig. 4(a)]. At the same time, the MD predicted transition appears sluggish, especially for the fully occupied case for which full densification of the amorphous form is not attained below 3 GPa. The reason for the sluggish transition and the discrepancy to the experimentally observed amorphization may be found in the PDFs.

Figure 7 depicts the evolution of PIA by comparing the PDFs for the fully occupied clathrate models. The rather abrupt transformation for AH at 1.7 GPa is seen with a

nonzero $g_{OO}(r)$ after the first coordination shell, $r > 3 \text{ \AA}$ (corresponding to four water molecules), and the liquidlike, rather featureless shape of $g_{OO}(r)$ beyond 4 \AA [Fig. 7(a)]. This coincides with the collapse of cages as seen with the $g_{OAr^H}(r)$ and $g_{OAr^D}(r)$. For the crystalline structure, before the collapse, the O-Ar contacts for the large H and small D cage are at about 4 and 3.7 \AA , respectively, whereas after the collapse, the contacts in both cages are at about 3.4 \AA [Figs. 7(b) and 7(c)]. The integrated coordination numbers for Ar^H and Ar^D attain a similar value out to 4.5 \AA , around 19, which indicates a similar hydration structure for both kinds of Ar atoms. For XH, the corresponding PDFs [shown in Figs. 7(d)–7(f)] reveal that PIA is a more continuous process, as already indicated in the density vs pressure behavior [cf. Fig. 6]. Molecular dynamics suggest amorphization at 2.5 GPa, which coincides with the appearance of a nonzero $g_{OO}(r)$ after the first coordination shell (in the range $r = 3\text{--}3.5 \text{ \AA}$), Fig. 7(d). However, the change of the XH $g_{OO}(r)$ at 2.5 GPa is not as abrupt as the one of the AH at 1.7 GPa [cf. Fig. 7(a)]. With increasing pressure, changes remain smooth. Specifically, the oscillating, crystalline feature after the first coordination shell is maintained up to 3 GPa. Eventually, at 4 GPa, the XH $g_{OO}(r)$ resembles that of AH after amorphization (i.e., at 1.7 GPa). The structural change at 2.5 GPa is most clearly seen from the evolution of $g_{OXe^T}(r)$ for which the first maximum shifts discontinuously from 3.8 to 3.7 \AA [Fig. 7(e)], indicating the collapse of large cages. At the same time, the coordination number for Xe^T remains very similar to that of the crystalline structure, and further changes only weakly up to 2.8 GPa. For the small (D) cages, O-Xe contacts are at $\sim 3.65 \text{ \AA}$ in the crystalline structure [Fig. 7(f)], which suggests repulsive interactions since the van der Waals radii for Xe and the O atom are 2.16 and 1.59 \AA , respectively [48]. The $g_{OXe^D}(r)$ functions look almost unchanged in the pressure range 2.3–3.0 GPa, which indicates that Xe atoms in the small cages maintain the ordered hydration environment of the crystalline structure.

From the PDF analysis, it can be inferred that PIA for XH proceeds very differently from AH. We interpret the change observed at 2.5 GPa as a transition to a semicrystalline state which is characterized by intact small cages and “collapsed” large cages in which Xe^T attains a disordered hydration environment but retains the coordination number from the crystalline structure. The further transition into the amorphous state is then a continuous process, which is completed above 4 GPa. During this process Xe atoms keep a quasi-ordered (periodic) arrangement which produces Bragg diffraction peaks. This picture is supported from MD snapshots, which are compiled in the SM [Fig. S2(a)] [29]. Note that, in contrast, during the discontinuous amorphization of CS-II AH, Ar atoms are moved significantly and irregularly from their crystalline equilibrium positions [Fig. S2(b)].

We then reexamined the diffraction patterns of XH [cf. Fig. 4(a)] with respect to the structural progression suggested by MD and included the diffuse scattering background, which should reveal an increasingly amorphized sample. A collection of these patterns is shown in Fig. 8 together with simulated diffraction patterns from MD snapshots at corresponding pressures. Indeed, one can notice an increased background when going from the 2.3 to the 3.4 GPa

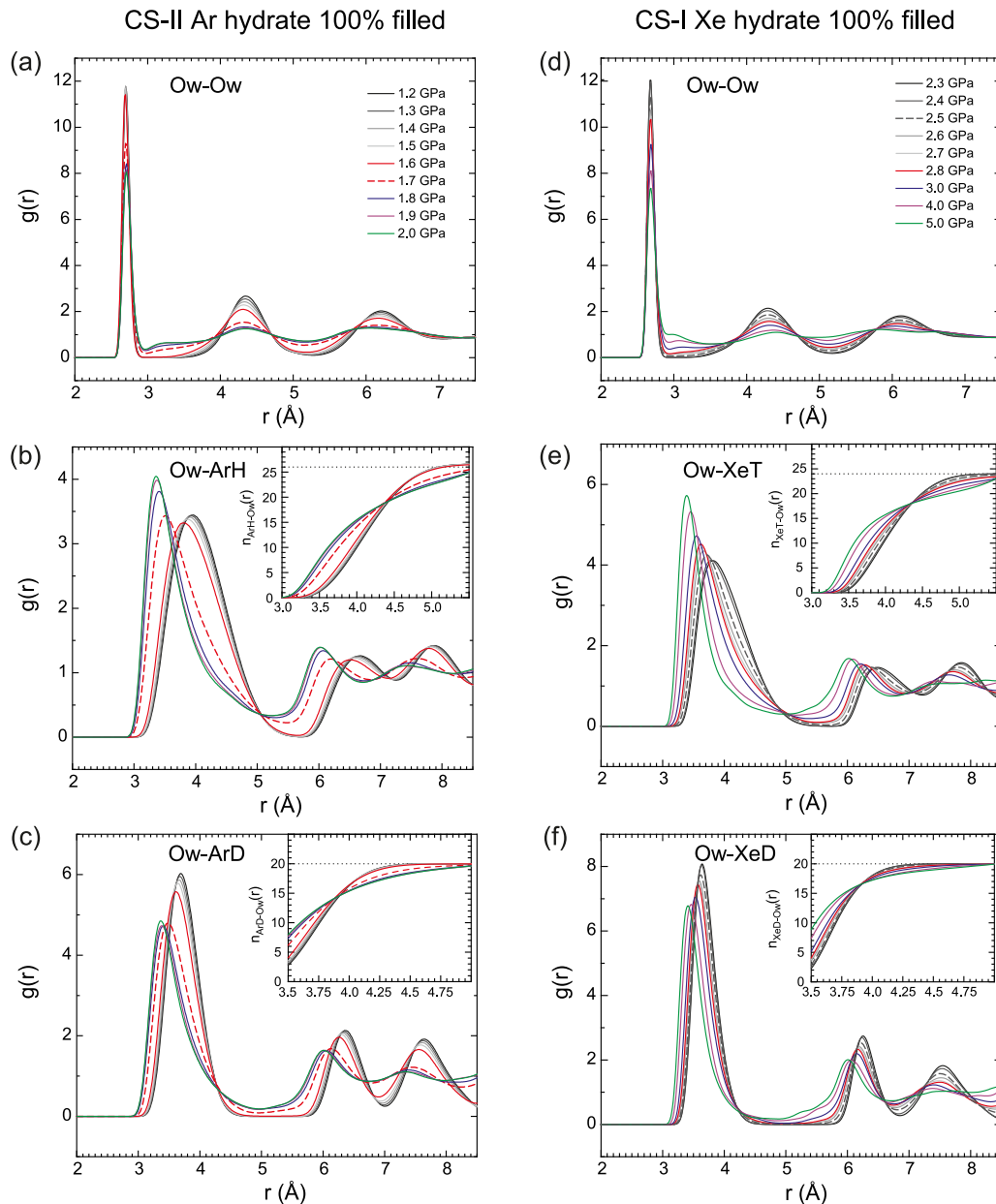


FIG. 7. Pressure dependence of the pair-distribution functions from the simulated molecular dynamics (MD) Ar and Xe hydrate systems at 95 K. (a) and (b) Oxygen-oxygen pair distribution functions (PDFs) from the water structures. (c)–(f) O-Ng PDFs with respect to guests inside small (D) and large (T and H) cages. The PDFs after transitions (crystalline \rightarrow amorphous and crystalline \rightarrow semicrystalline for Ar and Xe, respectively) are highlighted with broken lines. The insets in (b), (c) and (e), (f) show coordination numbers for (Ar^H, Ar^D) and (Xe^T, Xe^D), respectively.

pattern, and one may still discern weak Bragg features in the 4.5 GPa pattern. We note the good agreement with the simulated patterns, confirming that semicrystalline and a progressively amorphous state still give rise to Bragg diffraction peaks.

Figure 9 shows the major structural features of AH and XH [Figs. 9(a) and 9(b)] prior and after their amorphization and transition to the semicrystalline state, respectively [Figs. 9(c) and 9(d)]. It is seen that the densification of clathrate hydrate affects especially the larger hexagon rings of the H (CS-II) and T (CS-I) cages, whereas pentagon rings of the D cages maintain a rigid structure. A similar observation was made for CS-II THF hydrate with only H cages occupied [49]. The de-

formation of six-membered rings indicates (or triggers) onset of amorphization or transition. Concomitant with the onset of discontinuous densification, the Ng guest vibrational motion appears substantially hindered. Actual amorphization of CS-II AH is then characterized by an increasing distortion of pentagon rings, leading to the successive “collapse” of D cages [Fig. 9(c)]. At the same time, the coordination around both types of Ar atoms rearranges into that of the final amorphous state, which means that the hydration shells for the originally differently coordinated Ar guests even out. In contrast, apart from disordering, Xe guest atoms retain the hydration shell from the crystalline structure in the semicrystalline state up to 3 GPa [Fig. 9(d)].

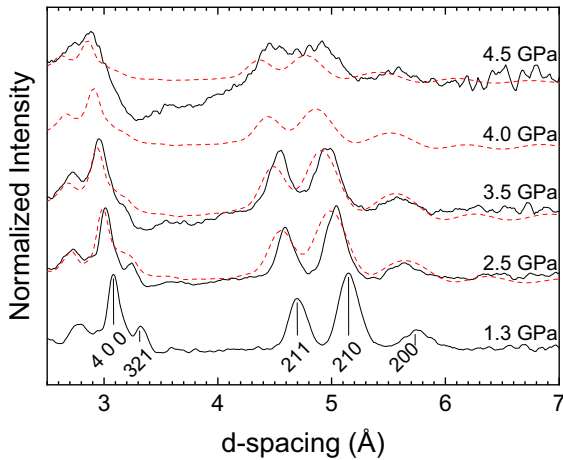


FIG. 8. Neutron powder diffraction (NPD) patterns showing the structural progression of CS-I Xe hydrate with pressure in experiments and molecular dynamics (MD) snapshots. Black lines represent experimental data (experiment XH2, SM [29]). Red-dotted lines represent simulated patterns from MD snapshots. Patterns show no sudden change in the long-range structure, and the final pattern with still crystalline features is in good agreement with experimental data.

C. Generalized PIA behavior for Ng clathrate hydrates from MD studies

We extend our study by looking generally at PIA behavior for Ng clathrate hydrates from MD studies. We first compare the Ng series for Ne to Xe for the two cubic structures, assuming fully occupied cages, i.e., $8Ng \cdot 46 H_2O$ for CS-I and $24Ng \cdot 136 H_2O$ for CS-II. The density-pressure relationships, referring to 95 K, and also including the empty clathrate structures, are shown in Fig. 10.

The empty clathrates amorphize at about 1.2–1.25 GPa, irrespective of the kind of cubic structure. This transition pressure is very similar to that of I_h , which has already been pointed out by Handa *et al.* [27]. The I_h -to-HDA transition from MD calculations is typically seen at 1.3–1.35 GPa for temperatures between 80 and 100 K [50,51]. Experimentally, it is observed at 1–1.1 GPa in this temperature range. Also, the completely filled clathrates, with stoichiometries $Ng \cdot 5.75 H_2O$ (CS-I) and $Ng \cdot 5.67 H_2O$ (CS-II), show a strikingly similar behavior irrespective of the kind of cubic structure. With increasing size of Ng, the amorphization pressure increases as 1.5 GPa (Ne), 1.6 GPa (Ar), and 1.9 GPa (Kr), with the peculiarity for Xe discussed in the previous section. Note that, for this generalized PIA discussion, we generically refer to a discontinuous density change as “amorphization,” as we did not analyze Kr hydrate and the partially filled model systems discussed below for a semicrystalline state.

To find out about the influence of the different cages, we next address different compositions in model systems referring to either fully occupied large (T and H) cages or fully occupied small (D) cages. If only the six T cages are occupied in CS-I, the composition is $Ng \cdot 7.67 H_2O$. If only the two D cages are filled, the composition is $Ng \cdot 23 H_2O$. With only H cages occupied, the composition for a CS-II

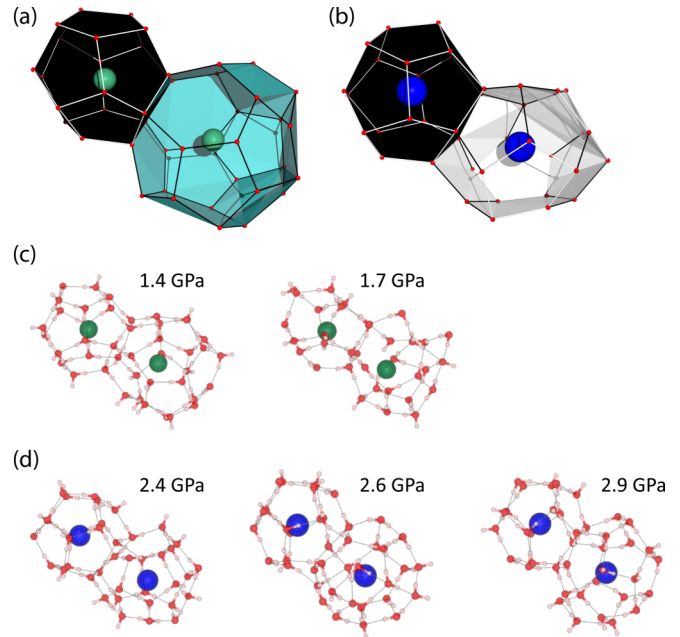


FIG. 9. Molecular dynamics (MD) snapshots showing the major structural features of Ar and Xe hydrate prior and after discontinuous densification at 95 K. (a) Crystalline CS-II Ar hydrate at 1.4 GPa. (b) Crystalline CS-I Xe hydrate at 2.0 GPa. (c) Guest environments in Ar hydrate at 1.4 GPa (crystalline) and 1.7 GPa (amorphous). (d) Guest environments in Xe hydrate at 2.4 GPa (crystalline) and 2.6 and 2.9 GPa (semicrystalline with disordered large cages). Red spheres: O, blue: Xe, green: Ar, white: H.

clathrate is $Ng \cdot 17 H_2O$, which is experimentally observed for, e.g., THF hydrate. If only D cages are occupied, then the composition is $Ng \cdot 8.5 H_2O$. CS-II Ne hydrate represents a special case since it assumes a more guest-rich composition of $Ng \cdot 4.25 H_2O$ with doubly occupied H cages [52], and this scenario is also included in our investigation.

The results are shown in Fig. 11. CS-I possesses a larger fraction of large cages T than CS-II. Only filling of minority cages stabilizes CS-I marginally, by 0.1 GPa for Ar and Kr and 0.2 GPa for (oversized) Xe [Fig. 11(a)]. A larger effect of the increasing size of Ng is seen when filling majority T cages. The amorphization pressure increases from 1.5 GPa (Ne) to 1.55 GPa (Ar) to 1.65 GPa (Kr) to 2 GPa for Xe. The stability of fully occupied CS-I [cf. Fig. 10(a)] is a cooperative effect of both T and D cage filling. CS-II possesses a larger fraction of small D cages than CS-I. Filling of minority H cages has no stabilizing effect with respect to empty CS-II, i.e., ice XVI [53], irrespective of the size of the Ng [Fig. 11(b)]. This agrees with the observation that, for CS-II clathrates, with rather large organic molecules, such as THF, 1,3-dioxolane, and cyclobutanone, for which only the large H cages are filled, the amorphization behavior is virtually identical [27,49]. Filling of the majority D cages has a clear stabilizing effect, which depends pronouncedly on the size of the Ng. The amorphization pressure is shifted to 1.5 GPa for Ne, to 1.6 GPa for Ar, to 1.8 GPa for Kr, which is closely mimicking the sequence of PIA pressures for the fully occupied case (Fig. 10). This indicates that small or majority cage filling almost solely determines the stability of CS-II hydrates with

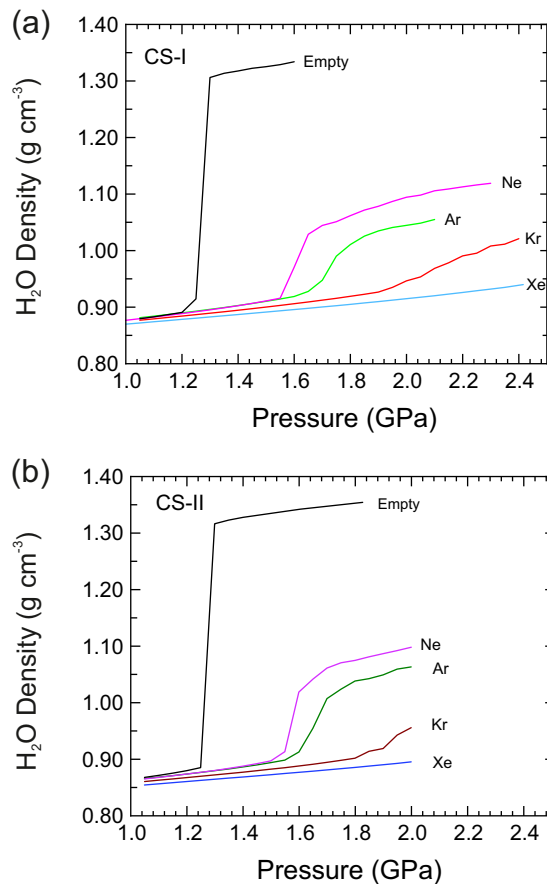


FIG. 10. Molecular dynamics (MD) derived density-pressure relations for (a) CS-I and (b) CS-II noble gas clathrate hydrates at 95 K. Both types of cages in each structure are completely filled, i.e., the compositions correspond to $\text{Ng} \cdot 5.75 \text{H}_2\text{O}$ for CS-I and $\text{Ng} \cdot 5.67 \text{H}_2\text{O}$ for CS-II.

respect to amorphization. The Ne case of doubly occupied H cages coherently mimics the behavior of a twice-as-large Ng (Ne $V_{\text{vdw}} = 15 \text{ \AA}^3$, Ar $V_{\text{vdw}} = 28 \text{ \AA}^3$, Kr $V_{\text{vdw}} = 35 \text{ \AA}^3$, Xe $V_{\text{vdw}} = 42 \text{ \AA}^3$) [48], with a collapse pressure at 1.7 GPa which is between that of Ar and Kr hydrate. Similarly, when D cages are empty and H cages remain doubly occupied, only a minor stabilization effect is observed.

IV. CONCLUSIONS

The high-pressure structural behavior of Ng clathrate hydrates was investigated at 95 K. As a general phenomenon, Ng clathrate hydrates undergo PIA at low temperatures, whereas at temperatures close to room temperature, crystal-crystal transitions to more guest-rich hydrate phases are observed [8–10,14,15,25]. Particularly, NPD experiments show that CS-II AH and CS-I XH amorphize at 1.4 and above 4 GPa, respectively. From MD simulations, it was concluded that, without a guest species, both cubic clathrate structures amorphize at 1.2 GPa, which is very similar to hexagonal ice. Filling of large-sized H cages does not provide stability toward amorphization for structure II, whereas filled small-sized dodecahedral D cages shift PIA to successively higher pressures with increasing size of the Ng guest. For CS-I, filling

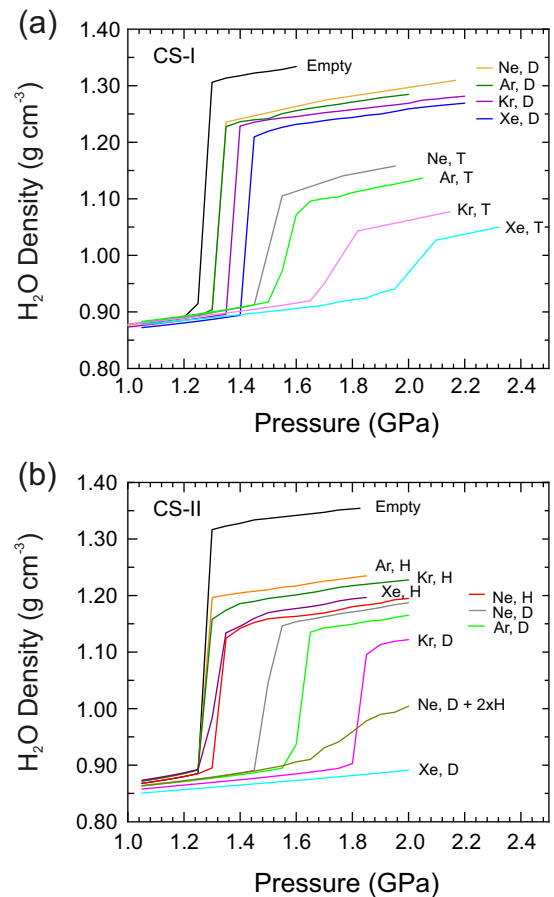


FIG. 11. Molecular dynamics (MD) derived density-pressure relations for CS-I and CS-II noble gas clathrate hydrates at 95 K considering different cage fillings. (a) Empty CS-I and Ne-Xe hydrate with only T or only D cages filled. (b) Empty CS-II (ice XVI) and Ne-Xe hydrate with only D or only H cages filled. CS-II Ne hydrate with only H cages doubly occupied (red line) and D cages singly occupied and H cages doubly occupied (olive line).

of both kinds of cages, large-sized T and small-sized D, acts to stabilize in a cooperative fashion. When fully occupied (referring to compositions $\text{Ng} \cdot 5.75 \text{H}_2\text{O}$ and $\text{Ng} \cdot 5.67 \text{H}_2\text{O}$ for CS-I and II, respectively), both cubic structures exhibit a similar behavior with PIA occurring in the pressure range of 1.3–2 GPa, depending on the size of the Ng. Xe represents a special case because it appears oversized as guest. Xe hydrate transforms at 2.5 GPa to a semicrystalline state in which the long-range order of Xe atoms and their water coordination numbers from the crystalline state are essentially retained. Continuous amorphization takes place above 3 GPa. We conjecture the similarity of Xe atom positions in the crystalline and amorphous state is the reason why amorphous XH recrystallized upon decompression in all recovery attempts. In contrast, amorphous CS-II AH is recoverable at ambient pressure when annealed at >1.5 GPa and 170 K.

ACKNOWLEDGMENTS

This research has been funded by the Swedish Foundation for Strategic Research (SSF) within the Swedish

national graduate school in neutron scattering (SwedNess). A portion of this research used resources at the Spallation Neutron Source, a DOE Office of Science User Facility operated by the Oak Ridge National Laboratory. The simulations were performed on resources provided by the Swedish National Infrastructure for Computing (SNIC)

at the National Supercomputer Centre (NSC). The authors also thank the financial support from eSSENCE, the Swedish Foundation for International Cooperation in Research and Higher Education (STINT), the Brazilian agency CAPES (Project CAPES/STINT N° 88887.304724/2018) and the Swedish Research Council (Registration No. 2019-05366).

- [1] E. D. Sloan Jr. and C. A. Koh, *Clathrate Hydrates of Natural Gases*, (CRC Press, Boca Raton, 2007).
- [2] J. H. van der Waals and J. C. Platteeuw, Clathrate solutions, in *Advances in Chemical Physics*, edited by I. Prigogine (John Wiley & Sons, Ltd, New Jersey, 2007).
- [3] G. A. Jeffrey, Hydrate inclusion compounds, *J. Incl. Phenom.* **1**, 211 (1984).
- [4] R. M. Barrer and W. I. Stuart, Non-stoichiometric clathrate compounds of water, *Proc. R. Soc. A* **243**, 172 (1957).
- [5] R. K. McMullan and G. A. Jeffrey, Polyhedral clathrate hydrates. IX. structure of ethylene oxide hydrate, *J. Chem. Phys.* **42**, 2725 (1965).
- [6] P. H. B. Brant Carvalho, A. Mace, O. Andersson, C. A. Tulk, J. Molaison, and U. Häussermann, Elucidating the guest disorder in structure II argon hydrate—a neutron diffraction isotopic substitution study, *J. Solid State Chem.* **285**, 121220 (2020).
- [7] C. A. Koh, Towards a fundamental understanding of natural gas hydrates, *Chem. Soc. Rev.* **31**, 157 (2002).
- [8] A. Y. Manakov, V. I. Voronin, A. V. Kurnosov, A. E. Teplykh, V. Y. Komarov, and Y. A. Dyadin, Structural investigations of argon hydrates at pressures up to 10 kbar, *J. Incl. Phenom.* **48**, 11 (2004).
- [9] J. S. Loveday and R. J. Nelmes, High-pressure gas hydrates, *Phys. Chem. Chem. Phys.* **10**, 937 (2008).
- [10] A. Y. Manakov, A. Y. Likhacheva, V. A. Potemkin, A. G. Ogienko, A. V. Kurnosov, and A. I. Ancharov, Compressibility of gas hydrates, *Chem. Phys. Chem.* **12**, 2476 (2011).
- [11] G. G. Malenkov, Argon and water, *J. Struct. Chem.* **54**, 252 (2013).
- [12] L. Yang, C. A. Tulk, D. D. Klug, I. L. Moudrakovski, C. I. Ratcliffe, J. A. Ripmeester, B. C. Chakoumakos, L. Ehm, C. D. Martin, and J. B. Parise, Synthesis and characterization of a new structure of gas hydrate, *Proc. Natl. Acad. Sci. USA* **106**, 6060 (2009).
- [13] Y. A. Dyadin, Clathrate formation in Kr-H₂O and Xe-H₂O systems under pressures up to 15 kbar, *Mendeleev Commun.* **7**, 74 (1997).
- [14] Y. A. Dyadin, Clathrate hydrate of xenon at high pressure, *Mendeleev Commun.* **6**, 44 (1996).
- [15] C. Sanloup, H. K. Mao, and R. J. Hemley, High-pressure transformations in xenon hydrates, *Proc. Natl. Acad. Sci. USA* **99**, 25 (2002).
- [16] A. Y. Manakov, V. I. Kosyakov, and S. F. Solodovnikov, Structural chemistry of clathrate hydrates and related compounds, in *Comprehensive Supramolecular Chemistry II* (Elsevier Inc., Amsterdam, 2017), Vol. 7, pp. 161–206.
- [17] Y. F. Makogon, Natural gas hydrates—a promising source of energy, *J. Nat. Gas Sci. Eng.* **2**, 49 (2010).
- [18] T. B. Peters, J. L. Smith, and J. G. Brisson, Production of CO₂ clathrate hydrate frozen desserts by flash freezing, *J. Food Eng.* **100**, 669 (2010).
- [19] X. Peng, Y. Hu, Y. Liu, C. Jin, and H. Lin, Separation of ionic liquids from dilute aqueous solutions using the method based on CO₂ hydrates, *J. Nat. Gas Chem.* **19**, 81 (2010).
- [20] A. G. Ogienko, E. V. Boldyreva, A. Y. Manakov, S. A. Myz, A. A. Ogienko, A. S. Yunoshev, E. G. Zevak, N. V. Kutaev, and A. A. Krasnikov, Preparation of fine powders of pharmaceutical substances by freeze-drying of frozen solutions in systems with clathrate formation, *Dokl. Phys. Chem.* **444**, 88 (2012).
- [21] A. Hassanpouryouzband, E. Joonaki, M. Vashghani Farahani, S. Takeya, C. Ruppel, J. Yang, N. J. English, J. M. Schicks, K. Edlmann, H. Mehrabian, Z. M. Aman, and B. Tohidi, Gas hydrates in sustainable chemistry, *Chem. Soc. Rev.* **49**, 5225 (2020).
- [22] W. L. Mao, C. A. Koh, and E. D. Sloan, Clathrate hydrates under pressure, *Phys. Today* **60**, 42 (2007).
- [23] R. Flacau, S. Desgreniers, and J. S. Tse, Electron density topology of cubic structure I Xe clathrate hydrate at high pressure, *J. Chem. Phys.* **129**, 244507 (2008).
- [24] L. Yang, C. A. Tulk, D. D. Klug, B. C. Chakoumakos, L. Ehm, J. J. Molaison, J. B. Parise, and J. M. Simonson, Guest disorder and high pressure behavior of argon hydrates, *Chem. Phys. Lett.* **485**, 104 (2010).
- [25] Y. A. Dyadin, E. G. Larionov, D. S. Mirinskij, T. V. Mikina, E. Y. Aladko, and L. I. Starostina, Phase diagram of the Xe-H₂O system up to 15 kbar, *J. Incl. Phenom. Mol. Recognit. Chem.* **28**, 271 (1997).
- [26] O. Mishima, Relationship between melting and amorphization of ice, *Nature* **384**, 546 (1996).
- [27] Y. P. Handa, J. S. Tse, D. D. Klug, and E. Whalley, Pressure-induced phase transitions in clathrate hydrates, *J. Chem. Phys.* **94**, 623 (1991).
- [28] H. Tanaka and Y. Amano, Pressure-induced amorphization of clathrate hydrates, *Mol. Phys.* **100**, 2183 (2002).
- [29] See Supplemental Material at <http://link.aps.org/supplemental/10.1103/PhysRevB.103.064205> for a description in detail of the neutron diffraction experiments and extra figures.
- [30] M. Matsumoto, T. Yagasaki, and H. Tanaka, GenIce: hydrogen-disordered ice generator, *J. Comput. Chem.* **39**, 61 (2018).
- [31] S. Plimpton, Fast parallel algorithms for short-range molecular dynamics, *J. Comput. Phys.* **117**, 1 (1995), See <http://lammps.sandia.gov> for information about the LAMMPS software.
- [32] J. L. F. Abascal, E. Sanz, R. G. Fernández, and C. Vega, A potential model for the study of ices and amorphous water: TIP4P/ice, *J. Chem. Phys.* **122**, 234511 (2005).
- [33] A. K. Rappé, C. J. Casewit, K. S. Colwell, W. A. Goddard, and W. M. Skiff, UFF, a full periodic table force field for molecular

- mechanics and molecular dynamics simulations, *J. Am. Chem. Soc.* **114**, 10024 (1992).
- [34] S. Melchionna, G. Ciccotti, and B. L. Holian, Hoover NPT dynamics for systems varying in shape and size, *Mol. Phys.* **78**, 533 (1993).
- [35] V. S. Neverov, XaNSoNS: GPU-accelerated simulator of diffraction patterns of nanoparticles, *SoftwareX* **6**, 63 (2017).
- [36] T. Ikeda-Fukazawa, Y. Yamaguchi, K. Nagashima, and K. Kawamura, Structure and dynamics of empty cages in xenon clathrate hydrate, *J. Chem. Phys.* **129**, 224506 (2008).
- [37] O. Andersson, P. H. B. Brant Carvalho, Y. J. Hsu, and U. Häussermann, Transitions in pressure-amorphized clathrate hydrates akin to those of amorphous ices, *J. Chem. Phys.* **151**, 014502 (2019).
- [38] Y. Suzuki, Evidence of pressure-induced amorphization of tetrahydrofuran clathrate hydrate, *Phys. Rev. B* **70**, 172108 (2004).
- [39] M. Bauer, D. M. Töbrens, E. Mayer, and T. Loerting, Pressure-amorphized cubic structure II clathrate hydrate: Crystallization in slow motion, *Phys. Chem. Chem. Phys.* **13**, 2167 (2011).
- [40] O. Andersson and G. P. Johari, Nature of the pressure-induced collapse of an ice clathrate by dielectric spectroscopy, *J. Chem. Phys.* **129**, 234505 (2008).
- [41] O. Andersson and Y. Nakazawa, Transitions in pressure collapsed clathrate hydrates, *J. Phys. Chem. B* **119**, 3846 (2015).
- [42] T. Loerting, C. Salzmann, I. Kohl, E. Mayer, and A. Hallbrucker, A second distinct structural 'state' of high-density amorphous ice at 77 K and 1 bar, *Phys. Chem. Chem. Phys.* **3**, 5355 (2001).
- [43] R. M. Barrer and A. V. J. Edge, Gas hydrates containing argon, krypton and xenon: kinetics and energetics of formation and equilibria, *Proc. R. Soc. A* **300**, 1 (1967).
- [44] S. Klotz, G. Hamel, J. S. Loveday, R. J. Nelmes, and M. Guthrie, Recrystallisation of HDA ice under pressure by in-situ neutron diffraction to 3.9 GPa, *Z. Kristallogr.* **218**, 117 (2003).
- [45] J. R. MacDonald, Review of some experimental and analytical equations of state, *Rev. Mod. Phys.* **41**, 316 (1969).
- [46] V. Vinš, A. Jäger, S. Hielscher, R. Span, J. Hrubý, and C. Breitkopf, Temperature & pressure correlation for volume of gas hydrates with crystal structures sI & sII, in *EPJ Web of Conferences*, edited by P. Dančová (EDP Sciences, Saint Louis, 2017), Vol. 143, p. 02141.
- [47] A. Y. Manakov, A. G. Ogienko, M. Tkacz, J. Lipkowski, A. S. Stoporev, and N. V. Kutaev, High-pressure gas hydrates of argon: Compositions and equations of state, *J. Phys. Chem. B* **115**, 9564 (2011).
- [48] A. Bondi, van der Waals Volumes and Radii, *J. Phys. Chem.* **68**, 441 (1964).
- [49] P. H. B. Brant Carvalho, A. Mace, C. L. Bull, N. P. Funnell, C. A. Tulk, O. Andersson, and U. Häussermann, Elucidation of the pressure induced amorphization of tetrahydrofuran clathrate hydrate, *J. Chem. Phys.* **150**, 204506 (2019).
- [50] F. Martelli, N. Giovambattista, S. Torquato, and R. Car, Searching for crystal-ice domains in amorphous ices, *Phys. Rev. Mater.* **2**, 075601 (2018).
- [51] J. Engstler and N. Giovambattista, Heating- and pressure-induced transformations in amorphous and hexagonal ice: A computer simulation study using the TIP4P/2005 model, *J. Chem. Phys.* **147**, 74505 (2017).
- [52] K. A. Lokshin, Y. Zhao, D. He, W. L. Mao, H. K. Mao, R. J. Hemley, M. V. Lobanov, and M. Greenblatt, Structure and Dynamics of Hydrogen Molecules in the Novel Clathrate Hydrate by High Pressure Neutron Diffraction, *Phys. Rev. Lett.* **93**, 125503 (2004).
- [53] A. Falenty, T. C. Hansen, and W. F. Kuhs, Formation and properties of ice XVI obtained by emptying a type sII clathrate hydrate, *Nature* **516**, 231 (2014).
- [54] C. G. Salzmann, Advances in the experimental exploration of water's phase diagram, *J. Chem. Phys.* **150**, 060901 (2019).